

Maxi-anion channel and pannexin 1 hemichannel constitute separate pathways for swelling-induced ATP release in murine L929 fibrosarcoma cells

Md. Rafiqul Islam, Hiromi Uramoto, Toshiaki Okada, Ravshan Z. Sabirov and Yasunobu Okada

Am J Physiol Cell Physiol 303:C924-C935, 2012. First published 11 July 2012;
doi: 10.1152/ajpcell.00459.2011

You might find this additional info useful...

This article cites 60 articles, 34 of which you can access for free at:
<http://ajpcell.physiology.org/content/303/9/C924.full#ref-list-1>

Updated information and services including high resolution figures, can be found at:
<http://ajpcell.physiology.org/content/303/9/C924.full>

Additional material and information about *American Journal of Physiology - Cell Physiology* can be found at:
<http://www.the-aps.org/publications/ajpcell>

This information is current as of November 1, 2012.

Maxi-anion channel and pannexin 1 hemichannel constitute separate pathways for swelling-induced ATP release in murine L929 fibrosarcoma cells

Md. Rafiqul Islam,¹ Hiromi Uramoto,² Toshiaki Okada,¹ Ravshan Z. Sabirov,^{1,3} and Yasunobu Okada¹

¹Department of Cell Physiology, National Institute for Physiological Sciences, Okazaki, Japan; ²Department of Health and Nutrition, Jin-ai University, Echizen, Fukui, Japan; and ³Institute of Physiology and Biophysics, Uzbekistan Academy of Sciences, Tashkent, Uzbekistan

Submitted 27 December 2011; accepted in final form 6 July 2012

Islam MR, Uramoto H, Okada T, Sabirov RZ, Okada Y. Maxi-anion channel and pannexin 1 hemichannel constitute separate pathways for swelling-induced ATP release in murine L929 fibrosarcoma cells. *Am J Physiol Cell Physiol* 303: C924–C935, 2012. First published July 11, 2012; doi:10.1152/ajpcell.00459.2011.—The maxi-anion channel plays a classically recognized role in controlling the membrane potential through the chloride conductance. It also has novel functions as a regulated pathway for the release of the anionic signaling molecules ATP and excitatory amino acids from cells subjected to osmotic perturbation, ischemia, or hypoxia. Because hemichannels formed by pannexins and connexins have been reported to mediate ATP release from a number of cell types, these hemichannels may represent the molecular correlate of the maxi-anion channel. Here, we found that L929 fibrosarcoma cells express functional maxi-anion channels which mediate a major portion of swelling-induced ATP release, and that ATP released via maxi-anion channels facilitates the regulatory volume decrease after osmotic swelling. Also, it was found that the cells express the mRNA for pannexin 1, pannexin 2, and connexin 43. Hypotonicity-induced ATP release was partially suppressed not only by known blockers of the maxi-anion channel but also by several blockers of pannexins including the pannexin 1-specific blocking peptide ¹⁰Panx1 and small interfering (si)RNA against pannexin 1 but not pannexin 2. The inhibitory effects of maxi-anion channel blockers and pannexin 1 antagonists were additive. In contrast, maxi-anion channel activity was not affected by pannexin 1 antagonists and siRNAs against pannexins 1 and 2. Although a connexin 43-specific blocking peptide, Gap27, slightly suppressed hypotonicity-induced ATP release, maxi-anion channel activity was not affected by Gap27 or connexin 43-specific siRNA. Thus, it is concluded that the maxi-anion channel is a molecular entity distinct from pannexin 1, pannexin 2, and connexin 43, and that the maxi-anion channel and the hemichannels constitute separate pathways for swelling-induced ATP release in L929 cells.

maxi-anion channel; pannexin; connexin; hemichannel; ATP release

THE MAXI-ANION CHANNEL belongs to a group of volume-regulated Cl[−] channels and is characterized by a large unitary single-channel conductance of approximately 300–400 pS, sensitivity to Gd³⁺ and arachidonic acid, and a ubiquitous expression pattern (33, 46). The channel has been observed from the very beginning of the patch-clamp era, but its activity was initially considered to be nonphysiological due to its exceedingly large amplitude. Recently, the maxi-anion channel has attracted a great deal of attention because of its permeability to anionic metabolites such as glutamate and ATP (45, 46). Studies on acutely isolated macula densa plaques (4), cultured (14) or freshly isolated (12) cardiomyocytes, and

cultured astrocytes (23–25) have demonstrated that the channel mediates the physiologically and pathophysiologically relevant release of ATP and glutamate. It therefore plays a vital role in the cell-to-cell purinergic and glutamatergic signal transduction that results in cardioprotection or neurodegeneration, depending on the target cell type and the nature of the activating stimulus.

Despite a long history of research and the important functions that have been attributed to the maxi-anion channel, the channel's molecular nature remains to be clarified. A mitochondrial voltage-dependent anion channel (VDAC or porin) expressed in the plasma membrane had long been under consideration as a molecular entity corresponding to the maxi-anion channel (42). However, the channel's activity was insensitive to genetic manipulations that eliminated the expression of the *Vdac1*, *Vdac2*, and *Vdac3* genes both individually and collectively (47), refuting this attractive hypothesis. Suzuki and Mizuno (54) and Suzuki (55) identified *Ttyh* genes in the human genome as possible candidates for the maxi-anion channel; these genes are homologous to the *Tweety* gene at the *Drosophila flightless* locus known to be involved in normal flying (31). However, a maxi-anion channel-like activity could not be detected in HEK293T cells transfected with two splice-variant clones, TTYH1-E and TTYH1-SV, of the TTYH1 gene (33).

Recently, connexins and pannexins have been proposed to serve as pathways for ATP release in the form of hemichannels (11, 30, 48, 59). In the present study, we therefore addressed the questions of whether pannexins or connexins are related to the maxi-anion channel and whether they participate in the swelling-induced ATP release in murine fibrosarcoma L929 cells.¹

MATERIALS AND METHODS

Cells. Murine L929 fibrosarcoma cells were obtained from Dr. Koh Ono (Kyoto University, Kyoto, Japan). The cells were cultured in RPMI 1640 medium (Nissui Pharmaceutical, Tokyo, Japan) supplemented with 0.1 mg/ml streptomycin, 40 U/ml penicillin, and 10% fetal bovine serum (FBS) (Equitech-Bio, Kerrville, TX; or Biowest, Nuaille, France) for all experiments. Mouse mammary fibroblast C127 cells were cultured in high glucose Dulbecco's modified Eagle's medium (DMEM) supplemented with 200 mg/l penicillin (Meiji Seika, Tokyo, Japan), 100 mg/l streptomycin (Meiji Seika), and 10% FBS and used only for DNA microarray analysis as the control. Cells were maintained at 37°C in a 5% CO₂ incubator and were usually split every 3–4 days.

Chemicals. Adenosine 5'-triphosphate disodium salt (ATP), 5-nitro-2-(3-phenylpropylamino)-benzoate (NPPB), arachidonic acid (arachidonate), probenecid, mefloquine, brefeldin A, apyrase (grade I), 1-octanol, Na-HEPES, EGTA, CsCl, and CsOH were purchased from

Address for reprint requests and other correspondence: Y. Okada, Dept. of Cell Physiology, National Institute for Physiological Sciences, Myodaiji-cho, Okazaki 444-8585, Japan (e-mail: okada@nips.ac.jp).

¹This article is the topic of an Editorial Focus by George R. Dubyak (11a).

Sigma-Aldrich (St. Louis, MO). Tyrphostin A23 (AG18) was purchased from TOCRIS Biosciences (Bristol, UK). GdCl₃ and bafilomycin A1 were purchased from WAKO (Osaka, Japan). HEPES was obtained from DOJINDO (Kumamoto, Japan). The pannexin 1 mimetic blocking peptide (WRQAAFVDSY)¹⁰Panx1 and the connexin 43 (Cx43) mimetic blocking peptide (SRPTEKTIFII) Gap27 were from AnaSpec (Fremont, CA).

Solutions. Normal Ringer solution was composed of (in mM): 135 NaCl, 5 KCl, 2 CaCl₂, 1 MgCl₂, 5 Na-HEPES, 6 HEPES, and 5 glucose (pH 7.4, 290 mosmol/kgH₂O). Artificial intracellular solution contained (in mM): 140 KCl, 5 HEPES, 5 EGTA, 1 MgCl₂, and 2.543 CaCl₂ (pH 7.4, adjusted with KOH; 294 mosmol/kgH₂O; pCa 7.0). For measurements of ATP permeability, a 100 mM Na₄ATP solution (pH 7.4 adjusted with NaOH) was used as the bath solution. ATP-containing solutions were kept on ice and warmed to room temperature immediately before each experiment. For inside-out patch-clamp experiments, the pipette was filled with normal Ringer solution, and the bath contained normal Ringer solution, the artificial intracellular solution, or the 100 mM Na₄ATP solution. In whole cell patch-clamp experiments, the pipette solution was composed of (in mM): 135 CsCl, 5 HEPES, 10 EGTA, 1 MgCl₂, and 2 CaCl₂ (pH 7.4 adjusted with CsOH; 280 mosmol/kgH₂O), and the bath contained normal Ringer solution. For outside-out patch-clamp experiments, the pipette solution contained (mM): 120 NaCl, 5 KCl, 5 HEPES, 10 EGTA, 1 MgCl₂, and 2 CaCl₂ (pH 7.4 adjusted with NaOH; 275 mosmol/kgH₂O), and the bath contained normal Ringer solution. In experiments with inhibitors or blockers, the stock solutions were prepared in DMSO and were diluted to their final concentrations immediately before the experiments. The final DMSO concentration did not exceed 0.1%, and DMSO did not have any effect when added alone. GdCl₃ was stored as a 50 or 500 mM stock solution in water. The stock solutions of the Panx1 and Cx43 mimetic blocking peptides (10 mg/ml) were prepared in water. For the ATP release assay, we used an isotonic 50 mM NaCl Ringer solution containing (in mM): 50 NaCl, 5 KCl, 2 CaCl₂, 1 MgCl₂, 5 Na-HEPES, and 6 HEPES (pH 7.4; 290 mosmol/kgH₂O adjusted with mannitol). In the hypotonic 50 mM NaCl solutions, only the amount of mannitol was varied so that the osmolality could be changed while keeping the ionic strength at a constant level, an essential condition for reproducibility of ATP measurements. Osmolality of all experimental solutions was measured with a freezing-point depression osmometer (OM802; Vogel, Kev-laer, Germany).

Electrophysiology. For inside-out and outside-out patch-clamp experiments, L929 cells were grown on glass coverslips for 1 day before the experiments. For whole cell experiments, suspensions of spherical cells were prepared by detaching them from the plastic substrate and culturing them with agitation. All patch-clamp recordings were carried out at room temperature (23–25°C). Patch pipettes were pulled from borosilicate glass capillaries (outer diameter 1.4 mm, inner diameter 1.0 mm) with a micropipette puller (model P-97; Sutter Instruments, Novato, CA) and had a tip resistance of ~2 MΩ when filled with the pipette solution. For whole cell recordings, the access resistance did not exceed 5 MΩ and was always compensated for (by 70–80%). Fast and slow capacitive transients were routinely compensated for. Single-channel recordings were made using the excised, inside-out or outside-out configuration of the patch-clamp technique. Membrane currents were measured with an Axopatch 200A patch-clamp amplifier coupled to a Digidata 1320 interface (Axon Instruments, Union City, CA). The time course of current change was monitored by repetitively applying (every 5 s) alternating step pulses (500-ms duration) to ±25 mV from a holding potential of 0 mV. To observe voltage dependence of the current profile, step pulses were applied with command voltages up to ±50 mV in 10-mV increments. Data acquisition and analysis were done with pClamp software (version 9.0.2; Axon Instruments) and WinASCD software (kindly provided by Dr. G. Droogmans, KU Leuven, Belgium). The membrane potential was controlled by shifting the pipette potential (V_p)

and reported as V_p for whole cell and outside-out recordings and $-V_p$ for inside-out recordings. Current signals were filtered at 2 kHz and digitized at 5 kHz. The liquid junction potentials were calculated with pCLAMP software and corrected when necessary. When the bath Cl⁻ concentration was changed, a salt bridge containing 3 M KCl in 2% agarose was used to minimize the bath electrode potential variation.

Luciferin-luciferase ATP assay. Hypotonicity-induced ATP release was quantified by a luciferin-luciferase assay system (ATP Luminescence Kit AF-2L1; DKK-TOA, Tokyo, Japan), as described previously (25). Briefly, L929 fibrosarcoma cells were cultured to confluence in 12- or 24-well plates. The 12-well plates were used for studies on osmolality and time dependence. Pharmacological studies were carried out using 24-well plates. After the culture medium was fully replaced with isotonic 50 mM NaCl Ringer solution (1,000 μl and 500 μl for 12- and 24-well plates, respectively), cells were incubated at 37°C for 60 min. To measure the background ATP release, an aliquot (100 μl) of the extracellular isotonic solution was collected and used as a reference sample. An osmotic challenge (124–290 mosmol/kgH₂O) was then applied by gently removing most of the remaining extracellular solution (875 μl and 300 μl for 12- and 24-well plates, respectively), adding the hypotonic 50 mM NaCl Ringer solution (1,000 and 400 μl for 12- and 24-well plates, respectively) and keeping the plates on a plate heater at 37°C. At specified time points, the plate was carefully rocked to ensure homogeneity of the extracellular solution, and samples (50 μl and 20 μl for 12- and 24-well plates, respectively) were collected from each well for the lumino-metric ATP assay. To the 20-μl samples that were collected, 30 μl of the 50 mM NaCl hypotonic solution was added to adjust the final volume to 50 μl, and 500 μl H₂O was added to make the final volume 550 μl. After addition of 50 μl of luciferin-luciferase reagent, measurements of the ATP concentration in the samples, all of equal ionic strength, were made with an ATP analyzer (model AF-100; DKK-TOA). For pharmacological studies, AG18 and other drugs were added to the isotonic and hypotonic solution, respectively, to their final concentration. The luciferin-luciferase assay mixture was supplemented with 600 μM EDTA when the samples contained Gd³⁺, because Gd³⁺ is known to interfere with the luciferin-luciferase reaction, as reported previously (5). The assay was calibrated using a standard 100 nM ATP solution free of, or containing, drugs. The drugs investigated in the present study had no significant effect on the luciferin-luciferase reaction system.

ATP release after siRNA-mediated gene knockdown was tested in 96-well plates 3 days after transfection. In some experiments, effects of probenecid and Gd³⁺ on ATP release were also observed in the cells cultured in 96-well plates. The cells were washed twice with the isotonic 50 mM NaCl Ringer solution using the automated Cell-WASHER APW-2000 (Ikeda Scientific, Tokyo, Japan) and incubated at room temperature for 30 min. The Ringer solution was then aspirated, and 100 μl of a test solution, composed of the isotonic or hypotonic 50 mM NaCl Ringer solution mixed with the luciferin-luciferase reagent in a ratio of 9:1, was slowly added to each well. Cells were incubated for 30 min at 37°C, and the luminescence intensity was measured using a luminescence microplate reader (CentroPRO LB962; Berthold Technologies, Bad Wildbad, Germany). The extracellular solution was then replaced with 50 μl of Hoechst33342 (Hoechst, Frankfurt, Germany) dissolved in normal Ringer solution, and Hoechst33342-stained nuclei were counted with the InCell Analyzer 1000 system (GE Healthcare, Little Chalfont, UK). The total luminescence intensity (in arbitrary units) for each well was normalized by the cell number to meet the variability in cell number per well after siRNA treatment.

Cell volume measurement. The mean cell volume was measured at room temperature using an electronic Coulter-type cell size analyzer (CDA-500; Sysmex, Kobe, Japan). Trypsinized L929 cells were suspended in either the isotonic or the hypotonic (124 mosmol/kgH₂O) 50 mM NaCl Ringer solution, and the mean cell volume was measured until 50 min.

Ethidium uptake measurement. The L929 cells were cultured to confluence in 96-well plates for 1 day at 37°C. Culture medium was fully replaced with 50 μ l isotonic 50 mM NaCl Ringer solution in the absence or presence of probenecid (1 mM) or Gd^{3+} (50 μ M) and incubated at 37°C for 30 min. The isotonic solution was then replaced with 50 μ l of high- K^+ hypotonic solution (50 mM KCl-based Ringer solution, 124 mosmol/kg H_2O with or without probenecid or Gd^{3+}) supplemented with 5 μ M ethidium bromide. The fluorescence was measured after 15 min at 37°C using Fluorescence Microplate Reader (Molecular Devices, Sunnyvale, CA) with the excitation/emission filter of 544/590 nm. After subtracting the background fluorescence which was measured in 96-well plates without cells, the fluorescence measured with cells was normalized to the control value measured at time zero just before application of the high- K^+ hypotonic solution.

Microarray analysis. DNA microarray analyses were carried out with Affymetrix GeneChip Mouse Gene 1.0 ST Arrays according to the standard Affymetrix protocol. Total RNAs were extracted from L929 and C127 cells using SEPAZOL (Nacalai Tesque, Kyoto, Japan), purified with the RNeasy Minikit (Qiagen, Hilden, Germany) and processed to cDNA (target) using the Ambion WT Expression Kit (Life Technologies, Carlsbad, CA) and the GeneChip WT Terminal Labeling and Controls Kit (Affymetrix, Santa Clara, CA). The raw CEL files were processed for gene-level analysis with median polish summarization and quantile normalization using Affymetrix Expression Console 1.1 software, and normalized intensity values were obtained. To identify up- or downregulated genes, we calculated Z-scores [z] and ratios (non-log scaled fold change) from the normalized intensity of each gene for comparisons between L929 cells, which were the experimental sample, and C127 cells, which were the control. Since an Affymetrix average difference (AD) level of 100 is thought to correspond to an extremely low or zero level of expression (53), we only considered genes for which there was an AD value >100. Microarray analysis support was provided by Cell Innovator (Fukuoka, Japan).

Small interfering RNA transfection. The murine L929 fibrosarcoma cells were transfected with small interfering (si)RNAs using a reverse-transfection method. Briefly, an aliquot (2–5 μ l) of siRNA solution (to yield a final concentration of 30 or 50 nM) was spread on the bottom of a 96-well culture plate, and 25 μ l of serum-free OPTI-MEM (GIBCO: Life Technology Japan, Tokyo, Japan) containing 0.75 μ l of the transfection reagent (Lipofectamine 2000; Invitrogen, Grand Island, NY) was added. After a 10-min incubation, the cells were seeded by adding 175 μ l of the cell suspension to give ~30% confluence on the day of transfection. Three to six hours after transfection, the cells were washed with RPMI plus 10% FBS culture medium and grown in the same medium for 2–4 days before patch-clamp and the ATP release assay. The siRNAs against the pannexins and connexin 43 were purchased from Sigma-Aldrich (*Panx1*, ID: SASI_Mm01_00066664 and *Panx2*, ID: SASI_Mm02_00286265) and Qiagen (*Gjal*, ID: Mm_Gjal_4). Fluorescence-labeled nontargeting siRNA (AllStars; Qiagen) was used as a negative control. The transfection efficiency was monitored under a fluorescence microscope. Nearly all L929 cells were observed to be successfully transfected under these experimental conditions.

RT-PCR. Molecular expression of the genes (*Panx1*, *Panx2*, and *Gjal*) in L929 cells and their knockdown by gene-specific siRNAs were monitored by RT-PCR. Total RNA was isolated from control or gene-specific siRNA-transfected cells using Sepasol RNA I reagent (Nacalai Tesque). Genomic DNA contamination of total RNA was removed by DNaseI treatment (RT-grade; Nippongene, Tokyo, Japan). cDNA was synthesized using an oligo(dT) primer (Invitrogen) and the GoScript Reverse Transcription System (Promega, Madison, WI). The sequences of the gene-specific primers were as follows: *Panx1*: forward, 5'-TCTTCTGGCGCTTCTTCTCTGC-3' and reverse, 5'-GGTCCAGGTCCGTCTCTTAGG-3' (product size 139 bp); *Panx2*: forward, 5'-GGAGCTCAACTTCCTTCTTCAG-3' and reverse, 5'-AGGTGGATGAGGTTGACTAGG-3' (product size 483

bp); and *Gjal* (*Cx43*): forward, 5'-TGCTCCTGGGGACAGCG-GTT-3' and reverse, 5'-TCCACGTTGACCCCGTCGGT-3' (product size 291 bp). Expression of GAPDH was monitored as an internal control. The sequences of the forward and reverse primers for GAPDH were 5'-ATGGTCTACATGTTCCAGT-3' and 5'-CCTTC-CACAATGCCAAAG-3', respectively (product size 392 bp). RT-PCR was carried out with a Gene Amp PCR System 9600 thermal cycler (Perkin-Elmer Life Sciences, Boston, MA) under the following cycling conditions: 10 min at 95°C (initial denaturation), 30–37 cycles of 1 min at 95°C, 2 min at 50°C (annealing) and 2 min at 72°C (elongation), and finally, 10 min at 72°C (final elongation).

Data analysis. Single-channel amplitudes were measured manually by placing a cursor at the open and closed channel levels. The mean patch currents were measured at the beginning (first 25–30 ms) of current responses to voltage steps to minimize the contribution of voltage-dependent current inactivation and the channel occupancy in subconductance states. Concentration-response data for Gd^{3+} -induced inhibition of the macropatch currents were fitted to the following equation:

$$I/I_o = 1/[1 + (X/K_d)^h] \quad (1)$$

where I_o and I are the currents in the absence and presence of Gd^{3+} at the concentration of X , respectively, K_d is the apparent dissociation constant, and h is the Hill coefficient. The concentration-response curve for Gd^{3+} -induced inhibition of the swelling-induced ATP release was fitted to the following equation:

$$A = (A_o - A_1)/[1 + (X/K_d)^h] + A_1 \quad (2)$$

where A_o and A are the levels of ATP released in the absence and presence, respectively, of Gd^{3+} at a concentration of X , A_1 is the noninhibited fraction of released ATP, K_d is the apparent dissociation constant, and h is the Hill coefficient. The ATP to Cl^- permeability ratio ($P_{\text{ATP}}/P_{\text{Cl}}$) was calculated from the Goldman-Hodgkin-Katz equation as described previously (41). Data were analyzed in OriginPro 7 (OriginLab, Northampton, MA). Plotted data are given as means \pm SE of n observations. Statistical differences of the data were evaluated by ANOVA, the Tukey honestly significant difference (HSD) test, and Student's t -test where appropriate and were considered significant at $P < 0.05$ or $P < 0.01$ as indicated.

In RT-PCR studies, the densitometric analysis of the amplified signal band was carried out using ImageJ software (National Institutes of Health, Bethesda, MD). Normalization was performed using the housekeeping gene *GAPDH*.

RESULTS

Activation of maxi-anion channel upon patch excision or protein tyrosine dephosphorylation. After membrane patches were excised from murine L929 fibrosarcoma cells, currents were found to be activated in the inside-out configuration in which the patches were exposed to normal Ringer solution applied in both the bath and pipette. A representative time course of channel activation is shown in Fig. 1A. The observed single-channel current amplitude was 10.5 ± 0.27 pA ($n = 10$) at +25 mV and -10.4 ± 0.26 pA ($n = 12$) at -25 mV, values which are close to the previously reported values in other cell types (46). After patch excision, the number of open channels increased with time and reached a steady-state level within 4–5 min, as shown in Fig. 1B. At the steady-state level, the opening of about 12 channels could be detected (data not shown, $n = 15$). In response to voltage steps, the steady-state maxi-anion channel currents showed voltage- and time-dependent inactivation kinetics, as illustrated in Fig. 1C. Voltage-dependent patch current inactivation occurred in a step-wise manner in which single-channel closing events could be observed. Such steady-state peak activation of the channels was found to

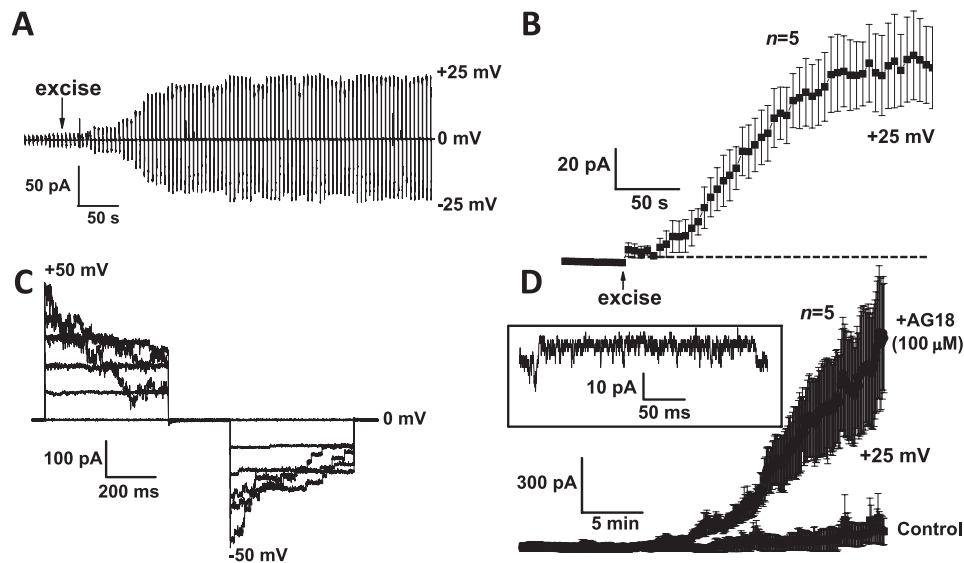


Fig. 1. Activation of maxi-anion channel currents in L929 cells. *A*: representative time course for maxi-anion channel activation after patch excision. The currents were recorded in the inside-out mode during repetitive application (every 5 s) of alternating test pulses (± 25 mV for 0.5 s) from the holding potential (0 mV). *B*: mean patch currents recorded at +25 mV as a function of time. Arrow indicates the time at which the patch was excised. *C*: voltage- and time-dependent inactivation of the steady-state membrane current in response to voltage pulses (500 ms) from holding at 0 mV to ± 50 mV in 10-mV increments. For *A* to *C*, the pipette and bath solutions were normal Ringer. *D*: activation of the maxi-anion channel macroscopic current after intracellular application of the tyrosine kinase inhibitor AG18 (100 μ M), under the whole cell configuration. The currents were recorded during application of ± 25 -mV test pulses. *Inset*: single maxi-anion channel-like events observed in the whole cell mode early after current activation. No drug was added to the pipette solution in control experiments. For *B* and *D*, each data point represents the mean \pm SE (vertical bar).

continue for the time period as long as 30 to 50 min, when the patch excision was performed in artificial intracellular solution added to the bath (data not shown; $n = 7$). Under the whole cell configuration, when the tyrosine kinase inhibitor AG18 was perfused intracellularly through the patch pipette, the macroscopic maxi-anion channel current was activated, even under normotonic conditions (Fig. 1*D*), as previously observed in other cell types (60). Single maxi-anion channel-like events

could be detected early in these whole cell records, as shown in the *inset* of Fig. 1*D*. These results demonstrate that murine L929 fibrosarcoma cells endogenously express maxi-anion channels, which can be activated upon membrane patch excision and tyrosine dephosphorylation.

Single-channel properties and ATP permeability of the maxi-anion channel. Figure 2*A* shows representative single-channel events occurring in response to step pulses applied

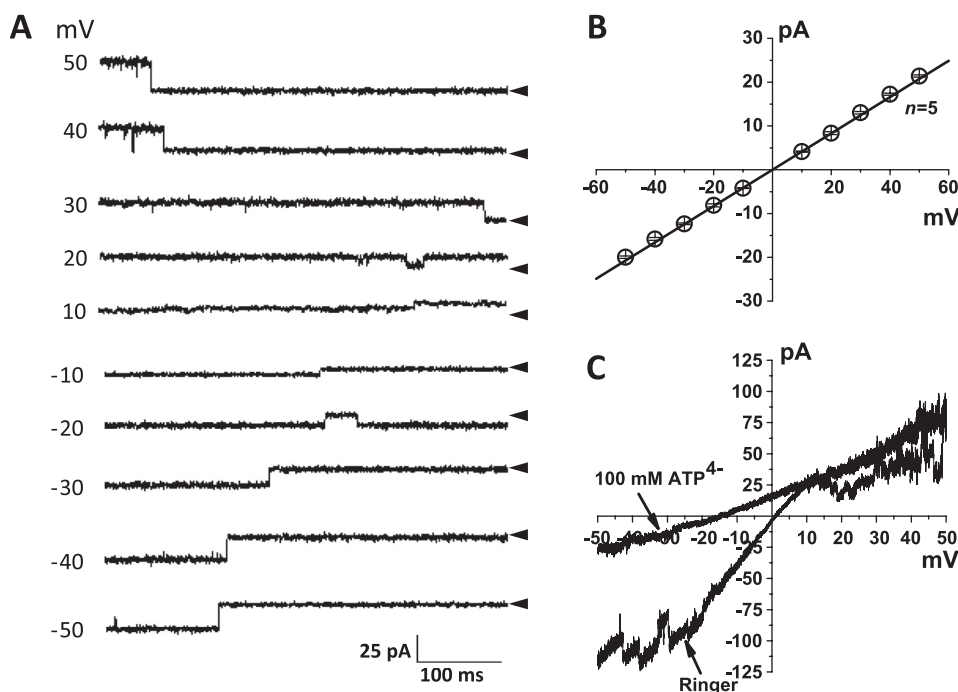
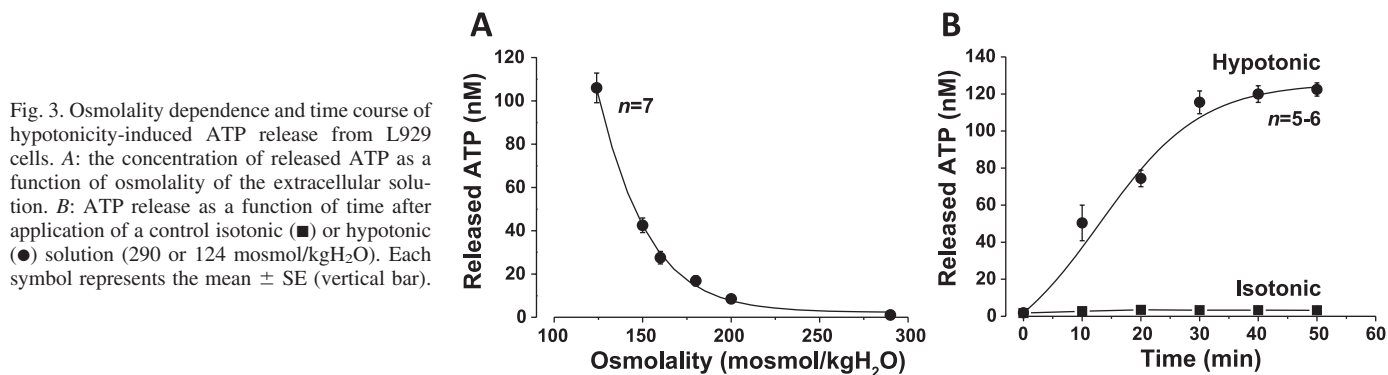


Fig. 2. Single-channel properties and ATP conductivity of the maxi-anion channel in inside-out membrane patches excised from L929 cells. *A*: representative current responses elicited by step pulses applied from a holding potential of 0 mV to the voltage levels indicated at the left of each trace. The pipette and bath were filled with normal Ringer solution. The arrowheads indicate the closed state. *B*: single-channel current-to-voltage (*I-V*) relationships for maxi-anion channel events recorded as in *A*. Each symbol represents the mean value \pm SE (vertical bar). The solid line is a linear fit with a slope conductance of 414.9 ± 4.9 pS. *C*: representative steady-state ramp *I-V* records from a macro-patch exposed to normal Ringer solution (Ringer) and 100 mM Na_4ATP solution (100 mM ATP^{4-}) in the bath. The pipette was filled with normal Ringer solution. The current recorded with ATP in the bath reversed at -14.9 ± 0.7 mV. A ramp pulse was applied from +50 to -50 mV at a rate of 25 mV/s.



from a holding potential of 0 mV to ± 50 mV in 10-mV increments. The channel currents exhibited time- and voltage-dependent inactivation at both positive and negative potentials greater than ± 20 mV. Under symmetrical chloride (Cl^-) conditions (with normal Ringer solution in the bath and pipette), the single-channel current-to-voltage (I - V) relationship was linear in the range of ± 50 mV and reversed at ~ 0 mV, as shown in Fig. 2B. The unitary slope conductance was 414.9 ± 4.9 pS ($n = 5$).

Since the maxi-anion channels in a number of cell types have been shown to exhibit significant ATP conductivity (44–46), we next tested the ATP conductivity of the maxi-anion channel in L929 cells. Under symmetrical ionic conditions with normal Ringer solution in both the pipette and bath, the steady-state I - V relationship determined with ramp pulses in macropatches containing multiple active channels appeared sublinear at voltages $> +15$ mV and more negative than -25 mV due to the voltage-dependent inactivation behavior, and the current reversed at 0 mV (Fig. 2C; Ringer). When all anions of the bath solution were replaced with 100 mM ATP^{4-} , the inward currents (presumably carried by ATP^{4-} from the bath solution) became smaller (Fig. 2C; 100 mM ATP^{4-}), and the reversal potential shifted to -14.9 ± 0.7 mV ($n = 5$), giving a $P_{\text{ATP}}/P_{\text{Cl}}$ value of 0.11 ± 0.01 . This value is similar to the values observed previously for other cell types (4, 14, 24, 41). These results indicate that this channel can act

as a gateway for the passage of signaling ATP molecules in fibrosarcoma cells.

Hypotonicity-induced ATP release from L929 cells. When L929 cells were incubated in normal Ringer solution, the concentration of extracellular ATP was 1.08 ± 0.21 nM ($n = 7$) after a 30-min incubation (Fig. 3A) and remained at a low level at least up to 50 min (Fig. 3B, filled squares). However, when the osmolality of the medium was decreased, the level of extracellular ATP gradually increased, reaching 106.0 ± 6.9 nM ($n = 7$) at 124 mosmol/kgH₂O (Fig. 3A). When cell swelling was induced by exposure to a hypotonic solution of 124 mosmol/kgH₂O, the concentration of released ATP increased in a time-dependent manner and reached a maximum level of approximately 120–125 nM within 30 min; the time course of ATP release had a sigmoidal shape with half-maximal ATP release observed at around 16 min (Fig. 3B, filled circles).

Sensitivity of maxi-anion channel currents and hypotonicity-induced ATP release to extracellular gadolinium. Gadolinium (Gd^{3+}) has been found to be a relatively specific inhibitor of swelling-induced ATP release (5, 40). Gd^{3+} can also potentially block the maxi-anion channel when it is applied from the extracellular, but not cytosolic, side (46). Therefore, we examined the concentration-dependent effects of Gd^{3+} on both maxi-anion channel currents recorded in the outside-out patch configuration and hypotonicity-induced ATP release in L929

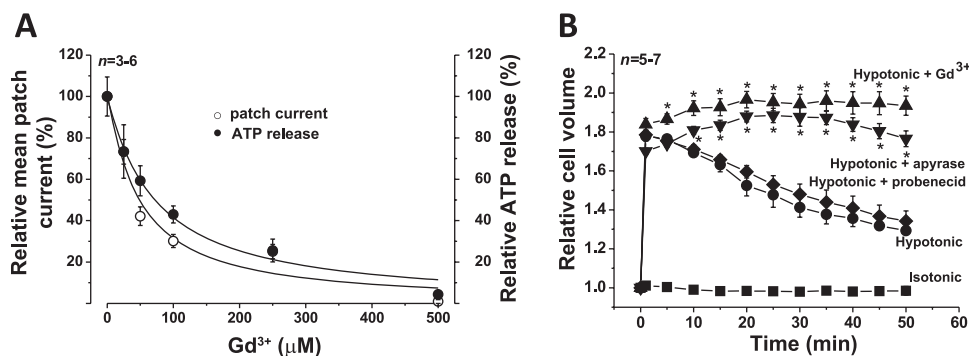


Fig. 4. Effects of gadolinium on the maxi-anion channel current, the hypotonicity-induced ATP release, and cell volume regulation in L929 cells. **A:** normalized mean patch current recorded from membrane patches in the outside-out configuration (\circ , $n = 3-6$) and normalized swelling-induced ATP release during hypotonic stress (124 mosmol/kgH₂O) (\bullet , $n = 5$), as a function of Gd^{3+} concentration. The data were fitted to the Hill equation, with $\text{IC}_{50} = 46 \pm 25$ μM for the currents and $\text{IC}_{50} = 73 \pm 11$ μM for ATP release. The Hill coefficients were 1.1 ± 0.7 and 1.1 ± 0.2 for the patch current and ATP release, respectively. Each symbol represents the mean \pm SE (vertical bar). **B:** effects of pyruvate (10 U/ml), Gd^{3+} (500 μM), or probenecid (1 mM) on regulatory volume decrease (RVD) in L929 cells. The relative mean cell volume was measured in either isotonic (\blacksquare) or hypotonic (\bullet) solution (290 or 124 mosmol/kgH₂O) and in hypotonic solution supplemented with pyruvate (\blacktriangledown), Gd^{3+} (\blacktriangle), or probenecid (\blacklozenge). Hypotonic stimulation was applied at time zero. Each data point represents the mean \pm SE (vertical bar). * $P < 0.05$ vs. hypotonic control. The mean cell volume was normalized to the initial value (observed at 0 min) with isotonic solution.

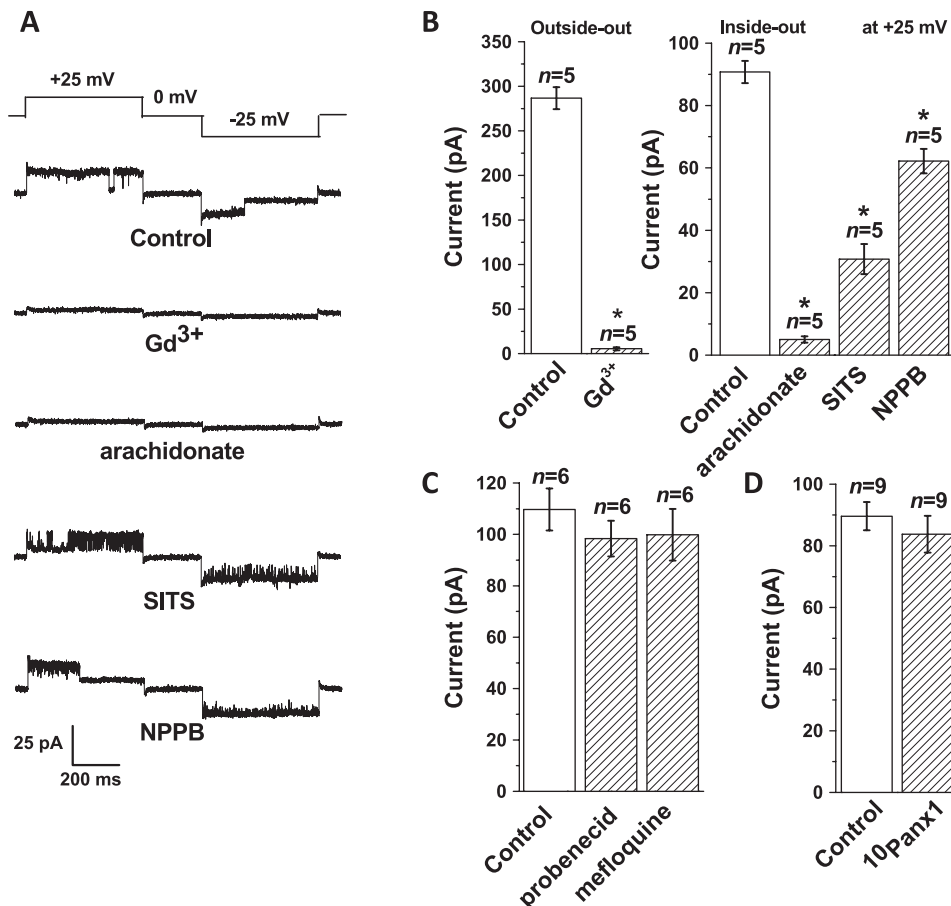


Fig. 5. Pharmacological profile of the maxi-anion channel currents in patches excised from L929 cells. **A**: representative single-channel current traces recorded in the inside-out mode [for arachidonic acid, SITS, and 5-nitro-2-(3-phenylpropylamino)-benzoate (NPPB), which were added from the intracellular side] or outside-out mode (for Gd³⁺, which was added from the extracellular side) in the absence (control) or presence of Gd³⁺ (500 μ M), arachidonate (20 μ M), SITS (100 μ M), or NPPB (100 μ M). The test pulse protocol is shown at the top. Recording conditions were as in Fig. 2. **B**: inhibitory effects of these drugs on the mean currents recorded at +25 mV in excised macropatches containing multiple maxi-anion channels. **C**: effects of the pannexin antagonists probenecid (1 mM) and mefloquine (0.1 μ M), added from the extracellular side, on the maxi-anion channel currents recorded in the inside-out mode. **D**: effect of the pannexin mimetic peptide ¹⁰Panx1 (8 μ g/ml) on the maxi-anion channel currents measured in the inside-out mode. The mimetic peptide was added from both the intracellular and the extracellular sides 8 min before and during recordings. Each column in **B–D** represents the mean \pm SE (vertical bar). * P < 0.05 vs. control.

cells. As shown in Fig. 4A (open circles), the mean steady-state patch current sharply decreased (by $\sim 70\%$) with an increase in the concentration of extracellular Gd³⁺ from 25 to 100 μ M, and it was nearly completely inhibited at a concentration of 500

μ M. An IC₅₀ of 46 ± 25 μ M and Hill coefficient of 1.1 ± 0.7 μ M were estimated for channel current inhibition by fitting the data to the Hill equation (Eq. 1). A similar concentration-response curve was observed when different concentrations of

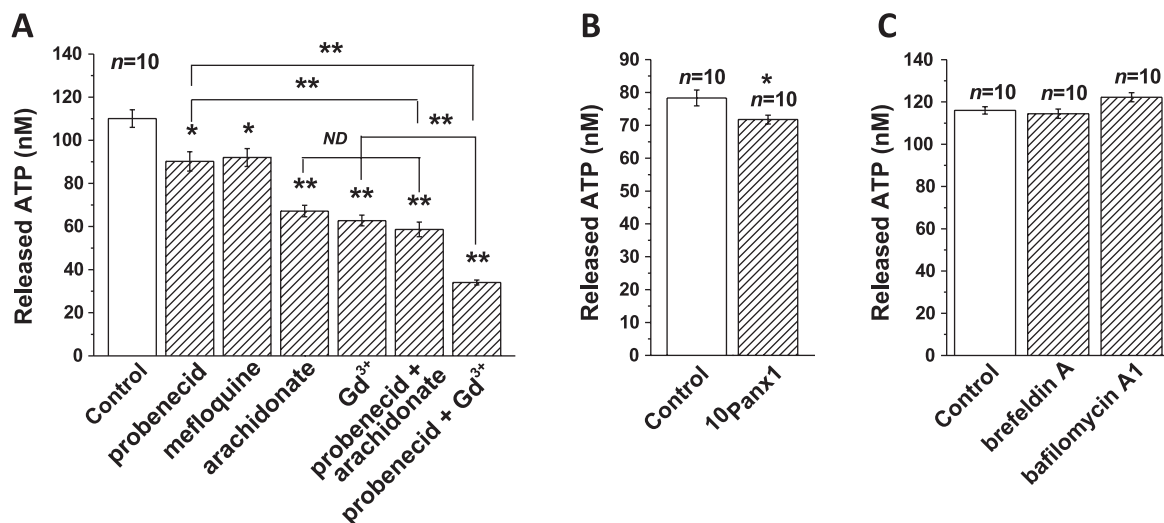


Fig. 6. Effects of antagonists of pannexin and the maxi-anion channel on hypotonicity-induced ATP release from L929 cells cultured in 24-well plates. Each column represents the mean \pm SE (vertical bar) ($n = 10$). All the values were corrected for the basal ATP release occurring under isosmotic conditions. * P < 0.05 vs. control; ** P < 0.01 vs. control or between two designated values. **A**: effects of the pannexin antagonists probenecid (1 mM) and mefloquine (0.1 μ M), and the maxi-anion channel antagonists Gd³⁺ (50 μ M) and arachidonate (40 μ M), on the ATP release occurring in response to hypotonic stimulation (124 mosmol/kgH₂O). ND, no significant difference. **B**: effect of the pannexin mimetic peptide ¹⁰Panx1 (8 μ g/ml) on the hypotonicity-induced ATP release from L929 cells. **C**: effects of brefeldin A (5 μ M) and bafilomycin A1 (5 μ M) on the ATP release from L929 cells.

Gd^{3+} were tested on the hypotonicity-induced ATP release from L929 cells (Fig. 4A, filled circles). An IC_{50} of $73 \pm 11 \mu\text{M}$ and Hill coefficient of $1.1 \pm 0.2 \mu\text{M}$ were obtained for ATP release inhibition by fitting the data to the Hill equation (Eq. 2). These data support the idea that the maxi-anion channel constitutes a major pathway for the swelling-induced release of ATP from fibrosarcoma cells. This inference was further supported by the observation that significant release of ATP could be evoked by treating the L929 cells with a tyrosine kinase inhibitor, AG18, even under isotonic conditions. In these experiments, the extracellular ATP concentration increased from $0.98 \pm 0.13 \text{ nM}$ ($n = 25$) to $2.12 \pm 0.26 \text{ nM}$ ($n = 25$; $P < 0.05$ vs. control) after 10-min incubation with AG18 ($100 \mu\text{M}$).

Facilitation of cell volume regulation by swelling-induced ATP release. L929 fibrosarcoma cells rapidly (within 1 min) responded to hypoosmotic stimulation ($124 \text{ mosmol/kgH}_2\text{O}$) with osmotic swelling, but restored their volume to $\sim 60\%$ after 50 min (Fig. 4B, circles), a process termed regulatory volume decrease (RVD). The RVD was almost completely inhibited by the removal of extracellular ATP with 10 U/ml apyrase or by addition of $500 \mu\text{M}$ Gd^{3+} (Fig. 4B, triangles). In contrast, probenecid (1 mM) failed to affect the RVD process (Fig. 4B, diamonds). These results suggest that swelling-induced ATP release plays a facilitatory role in the cell volume regulation in fibrosarcoma cells, and that the maxi-anion channel activity is critical for this process.

Insensitivity of maxi-anion channel currents to pannexin antagonists. Effects of a number of anion channel blockers on maxi-anion channel currents recorded at $\pm 25 \text{ mV}$ are shown in Fig. 5, A and B. Maxi-anion channel activity was drastically inhibited by Gd^{3+} and arachidonate, in agreement with observations in mammary C127 cells (13, 41), cardiac myocytes (14), and cultured astrocytes (24). The maxi-anion channel current was also partially sensitive to the conventional anion channel inhibitors SITS and NPPB (Fig. 5B), consistent with previous observations in other cell types (12, 14, 23, 41).

To test the possibility that the hemichannel function of pannexins underlies maxi-anion channel activity, we first tested the effects of the relatively specific pannexin hemichannel blockers probenecid (51) and mefloquine (20). As shown in Fig. 5C, neither probenecid (1 mM) nor mefloquine ($0.1 \mu\text{M}$) was effective in blocking the maxi-anion channel currents activated after patch excision from L929 cells. We then tested the effect of a pannexin mimetic peptide, $^{10}\text{Pannx1}$ ($8 \mu\text{g/ml}$), which specifically blocks pannexin 1 hemichannel activity (36), on the maxi-anion channel currents. However, the peptide did not have any suppressive effect on the maxi-anion currents, as shown in Fig. 5D. These pharmacological data strongly suggest that the maxi-anion channel is distinct from the pannexin 1 hemichannel.

Sensitivity of swelling-induced ATP release to maxi-anion channel blockers and pannexin antagonists. Functional expression of pannexin hemichannels in L929 cells was examined by the uptake of cationic dye, ethidium $^{+}$, under high- K^{+} hypotonic conditions, because the activity of pannexin 1 hemichannels monitored by cationic dye uptake is known to be stimulated by high- K^{+} -induced depolarization and/or hypotonicity (37, 50, 62). The ethidium fluorescence increased to $360.9 \pm 22.5\%$ ($n = 20$) 15 min after stimulation with high- K^{+} hypotonic solution. The ethidium uptake was significantly sup-

pressed to $220.3 \pm 23.7\%$ ($n = 19$) in the presence of the pannexin antagonist probenecid (1 mM), whereas the dye uptake (to $364.6 \pm 33.1\%$, $n = 18$) was not significantly affected by the maxi-anion channel blocker Gd^{3+} ($50 \mu\text{M}$). Thus, there arises a possibility that pannexins contribute to the swelling-induced release of ATP from the fibrosarcoma cells. We then tested the effect of probenecid, which can differentiate pannexins from connexins (29, 51), on hypotonicity-induced ATP release. As shown in Fig. 6A, 1 mM probenecid inhibited, by $\sim 18\%$, the ATP release from L929 cells. A similar extent of inhibition was observed for another relatively selective pannexin blocker, mefloquine ($0.1 \mu\text{M}$). Moreover, hypotonicity-induced ATP release was also inhibited by the pannexin mimetic peptide $^{10}\text{Pannx1}$ ($8 \mu\text{g/ml}$) (Fig. 6B). These findings suggest that pannexin 1 may represent one of the pathways for the ATP release that occurs upon a hypotonic challenge.

The contribution of the maxi-anion channel was tested by applying gadolinium and arachidonic acid. Arachidonate (40

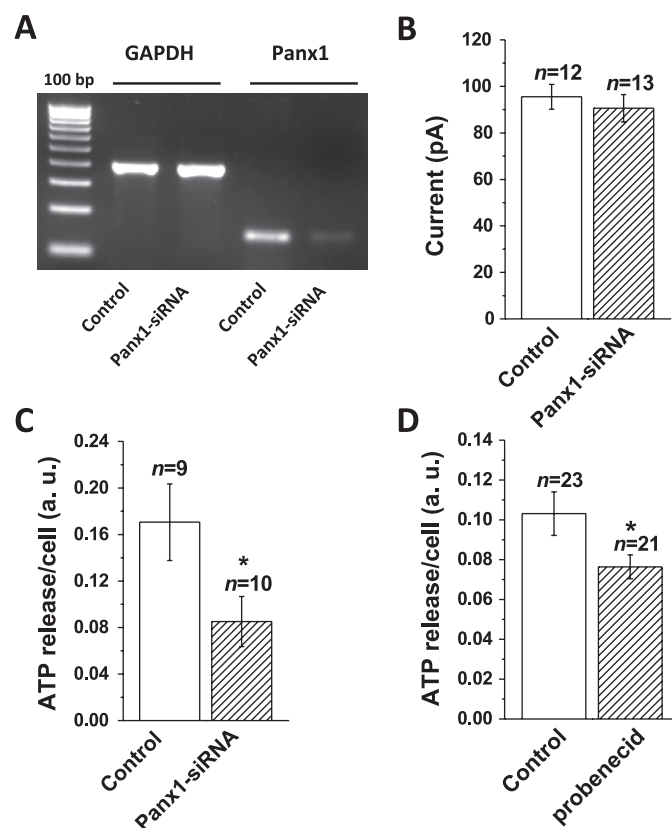


Fig. 7. Effects of small interfering (si)RNA-mediated knockdown of *Pannx1* expression on the maxi-anion channel currents and swelling-induced ATP release in L929 cells cultured in 96-well plates. Experiments were conducted 3 days after transfection with 30 nM siRNA. A: expression of *Pannx1* mRNA after treatment with nontargeting siRNA (control) or *Pannx1*-specific siRNA, analyzed by RT-PCR. GAPDH was used as an internal control. The mean inhibition of the *Pannx1* signal was 78.3% in triplicate experiments (estimated by densitometric analysis with normalization to the GAPDH signal). B: the mean maxi-anion channel currents observed at $+25 \text{ mV}$ in excised patches after transfection with the negative control or *Pannx1*-specific siRNA. C: ATP release induced by hypotonicity ($124 \text{ mosmol/kgH}_2\text{O}$) after siRNA treatment. The luminescence values [in arbitrary units (AU)] were normalized by the cell number after correcting for the basal ATP release occurring under isotonic conditions. * $P < 0.05$ vs. control. D: ATP release induced by hypotonicity in the absence or presence of probenecid (1 mM). * $P < 0.05$ vs. control.

μM) and Gd^{3+} (50 μM) inhibited hypotonicity-induced ATP release from L929 cells cultured in 24-well plates by approximately 39% and 43%, respectively (Fig. 6A). Gd^{3+} -induced inhibition (by $38.4 \pm 0.006\%$, $n = 20$) of swelling-induced ATP release was similarly observed in the cells cultured in 96-well plates. When probenecid was added together with arachidonate or Gd^{3+} , ATP release was further inhibited (Fig. 6A). Such additive effects imply that the maxi-anion channel and the pannexin hemichannel most likely constitute separate, individual pathways for the release of ATP in murine fibrosarcoma cells.

Recently, exocytosis has also been found to be one of the pathways contributing to some extent to the ATP release in bovine ciliary epithelial cells (26) as well as other cell types (1, 38, 56, 57). We tested this possibility by applying the exocytosis blockers brefeldin A (5 μM) and bafilomycin A1 (5 μM). However, neither of these drugs inhibited the hypotonicity-induced ATP release from L929 cells (Fig. 6C), suggesting that in fibrosarcoma L929 cells, exocytosis is not involved in ATP release.

Molecular expression pattern of pannexins and connexins in L929 cells analyzed by microarray. Before testing siRNA-mediated knockdown of specific genes, we verified the expression of pannexins and connexins by DNA microarray analysis. This analysis showed that pannexins 1 and 2 are moderately expressed while pannexin 3 is below the threshold expression level. So far, among a large number of connexin (Cx) family members, ATP release has been reported to be mediated by Cx43 (17, 35), Cx32 (9), and Cx26 (19). For L929 cells, a strong Cx43 signal was detected while signals for Cx32 and Cx26 were far below the threshold. These results indicate that L929 cells predominantly express Cx43. Based on the results from this high-throughput gene expression analysis, we then tested the effects of siRNA-mediated knockdown of pannexin 1, pannexin 2, and Cx43.

Insensitivity of the maxi-anion channel current and sensitivity of hypotonicity-induced ATP release to pannexin 1 and connexin 43 gene silencing. Transfection of L929 cells with *Panx1*-specific siRNA suppressed the expression of pannexin 1

mRNA by $\sim 78\%$ compared with the control nontargeting siRNA (mock), as shown in Fig. 7A. However, the amplitude of the mean patch current observed in *Panx1*-siRNA-transfected L929 cells was not significantly different from that observed in the mock-transfected control cells (Fig. 7B). This clearly indicates that the *Panx1* gene product is different from the maxi-anion channel. However, the hypotonicity-induced ATP release from L929 cells cultured in 96-well plates was significantly suppressed by *Panx1*-siRNA (Fig. 7C) and by probenecid (Fig. 7D). These results suggest that pannexin 1 serves as one of the pathways for swelling-induced ATP release from L929 cells, but that pannexin 1 and the maxi-anion channel are independent of each other.

Although treatment with *Panx2*-specific siRNA largely eliminated (by $\sim 94\%$) the expression of *Panx2* mRNA (Fig. 8A), neither maxi-anion channel activity (Fig. 8B) nor swelling-induced ATP release (Fig. 8C) was affected by this maneuver. These findings indicate that pannexin 2 is not involved in ATP release and also that it is distinct from the maxi-anion channel in L929 cells.

The general connexin hemichannel blocker 1-octanol had no significant effect on maxi-anion channel activity or swelling-induced ATP release (Fig. 9, A and B). The connexin 43 mimetic peptide Gap27 (15) had no effect on maxi-anion channel activity (Fig. 9B) but slightly decreased the swelling-induced ATP release (Fig. 9A). Connexin 43 (*Gja1*)-specific siRNA treatment largely suppressed (by $\sim 73\%$) the expression of connexin 43 mRNA (Fig. 9C) but had no effect on maxi-anion channel activity (Fig. 9D). The lack of any effect of 1-octanol, Gap27, or Cx43-specific siRNA on the maxi-anion channel currents indicates that connexin 43 and the maxi-anion channel are unrelated entities.

DISCUSSION

L929 cells functionally express the ATP-conductive maxi-anion channel. Under resting conditions, the maxi-anion channel normally remains in a dormant state; upon stimulation by several kinds of stimuli, it is activated in a large variety of cell

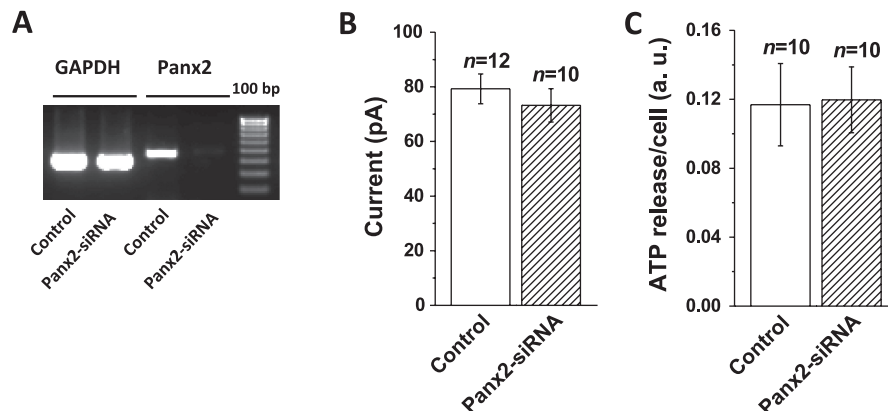


Fig. 8. Effects of siRNA-mediated knockdown of *Panx2* expression on the maxi-anion channel currents and swelling-induced ATP release in L929 cells. Experiments were conducted 3 days after transfection with 50 nM siRNA. A: expression of *Panx2* mRNA after treatment with nontargeting siRNA (control) or *Panx2*-specific siRNA, analyzed by RT-PCR. GAPDH was used as an internal control. The mean inhibition of the *Panx2* signal was 93.8% in duplicate experiments (estimated by densitometric analysis with normalization to the GAPDH signal). B: the mean maxi-anion channel currents observed at +25 mV in excised patches after transfection with the negative control or *Panx2*-specific siRNA. C: ATP release induced by hypotonicity (124 mosmol/kgH₂O) after siRNA transfection. The luminescence values (in AU) were normalized by the cell number after correcting for the basal ATP release occurring under isosmotic conditions.

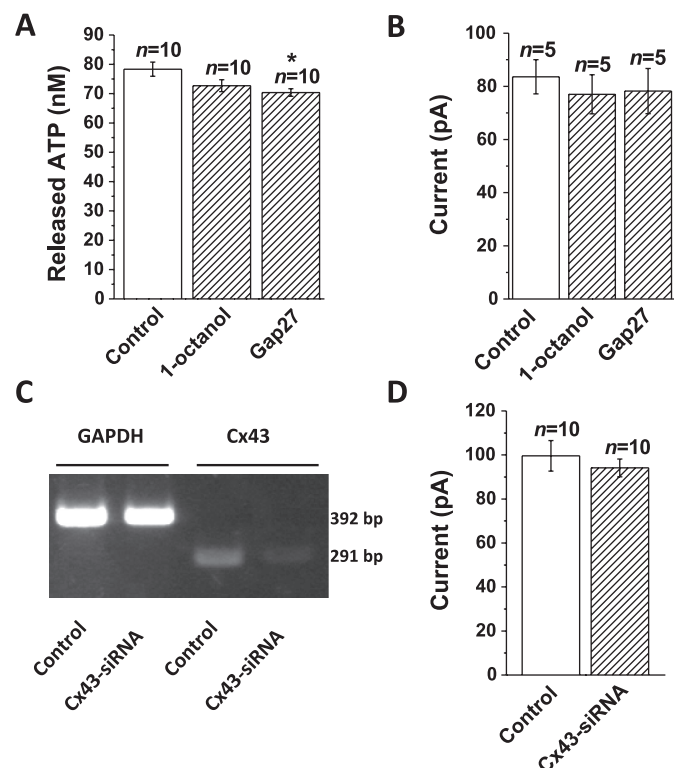


Fig. 9. Effects of the connexin inhibitor 1-octanol, the connexin 43 (Cx43) mimetic peptide Gap27 and *Gjal*-specific siRNA-mediated Cx43 knockdown on swelling-induced ATP release and/or the maxi-anion channel currents in L929 cells. **A:** ATP release induced by hypotonic stress (124 mosmol/kgH₂O) without drug treatment (control) and after a 20-min preincubation with 1-octanol (1 mM) or Gap27 (8 μ g/ml). **P* < 0.05 vs. control. **B:** excision-induced maxi-anion channel currents in the absence (control) or presence of 1-octanol (1 mM) or Gap27 (8 μ g/ml). For the Gap27 experiment, the cells were also preincubated with this peptide for 20 min. **C:** expression of *Gjal* (Cx43) mRNA in L929 cells treated with nontargeting (control) siRNA or *Gjal*-specific siRNA (Cx43-siRNA), 3 days after transfection (with 50 nM), analyzed by RT-PCR. GAPDH was used as an internal control. The mean inhibition of the connexin 43 signal was 72.8% in duplicate experiments (estimated by densitometric analysis with normalization to the GAPDH signal). **D:** effects of the negative control and *Gjal*-specific siRNA on the maxi-anion channel currents recorded at +25 mV. Each column in A, B, and D represents the mean \pm SE (vertical bar).

types (46). In our previous studies, we reported the activation of the maxi-anion channel in mammary C127i cells (41), astrocytes (25), and cardiomyocytes (12, 14) by osmotic cell swelling, in kidney macula densa cells by salt stress (4), and in cardiomyocytes and astrocytes by ischemia/hypoxia (14, 23, 24). Among all the activation stimuli used in these studies, patch excision was found to be the strongest. The mechanism of channel activation has not yet been completely clarified. However, a recent study by Toychiev et al. (60) showed that phosphorylation of tyrosine residues of the maxi-anion channel or a regulatory subunit keeps the channel in the closed state, and that upon patch excision, the channel is activated by protein tyrosine phosphatase-mediated dephosphorylation. In the present study, we observed a robust activation of the maxi-anion channel in L929 fibrosarcoma cells by both patch excision (in the inside-out mode) and intracellular application of the tyrosine kinase inhibitor AG18 (in the whole cell mode) (Fig. 1). The activated maxi-anion channel displayed a linear current-voltage (*I*-*V*) relationship, a large single-channel con-

ductance of ~ 415 pS, permeability to ATP⁴⁻ (Fig. 2), and sensitivity to Gd³⁺ and arachidonic acid (Fig. 5). These properties of the maxi-anion channels in L929 cells are identical to those observed in other cell types (46). Thus, it is concluded that the maxi-anion channel is endogenous to, and functional in, murine L929 fibrosarcoma cells.

Maxi-anion channel and pannexin 1 are separate, distinct entities. The maxi-anion channel and the recently characterized pannexin 1 hemichannel display the following overlapping properties: 1) both the maxi-anion channel (46) and pannexin 1 (11) are ubiquitously expressed; 2) both the maxi-anion channel (41) and pannexin 1 (39) are activated by osmotic cell swelling; 3) the pore radius of the maxi-anion channel is approximately 1.3 nm (43) and that of pannexin is approximately 1.7–2.1 nm (2); 4) the maxi-anion channel and pannexin 1 hemichannel have large single-channel conductances of approximately 300–450 pS (46) and 300–550 pS (3, 22, 58), respectively, with several subconductance states; 5) no rectification was reported for the maxi-anion channel (46) and little or no outward rectification was reported for the pannexin 1 hemichannel (3, 22, 30, 58); 6) both the maxi-anion channel (4, 14, 24, 41) and pannexin 1 hemichannel (3) are permeable to ATP; and 7) both the maxi-anion channel (12, 14, 23, 41) and pannexin 1 (29) are partially sensitive to SITS, NPPB and DIDS. Based on these similarities, we hypothesized that the pannexin 1 hemichannel could be the molecular correlate of the maxi-anion channel. However, we found that maxi-anion channel activity was not sensitive to known blockers of pannexin 1 such as probenecid, mefloquine, and ¹⁰Panx1 (Fig. 5). Microarray and RT-PCR data revealed low but detectable expression of pannexin 1 in L929 cells. However, we did not observe any difference in the maxi-anion channel currents recorded from mock- and *Panx1*-specific siRNA-transfected L929 cells despite a large decrease in mRNA expression due to *Panx1* siRNA transfection (Fig. 7). Based on these electrophysiological and pharmacological data we conclude that the maxi-anion channel and pannexin 1 hemichannel are separate, distinct entities. Our conclusion is supported by reported differences between the properties of these two channels which include the following: 1) the maxi-anion channel is inhibited by Gd³⁺ (46), whereas pannexin 1 is insensitive to it (29, 36); and 2) the maxi-anion channel is highly anion selective (45, 46), while the pannexin 1 hemichannel supposedly has a nonselective cation pore (3, 22, 58).

Hypotonicity-induced ATP release occurs via maxi-anion channels and pannexin hemichannels but not by exocytosis. The fibrosarcoma maxi-anion channel was found to be permeable to ATP, a prerequisite for its role as an ATP-conductive pathway. The sensitivity of the hypotonicity-induced ATP release from L929 cells to Gd³⁺ (Figs. 4 and 6) and arachidonic acid (Fig. 6) strongly suggests that a major portion of the released ATP passes through the fibrosarcomal plasmalemma via the maxi-anion channel. This result is consistent with our previous observations on the role of the maxi-anion channel in the release of ATP from mammary C127 cells (41), macula densa cells (4), cardiomyocytes (12, 14), and astrocytes (25). On the other hand, the functional expression of the pannexin hemichannels in L929 cells was indicated by the ethidium uptake

assay. The swelling-induced ATP release was partially suppressed by the pannexin hemichannel inhibitors probenecid and mefloquine as well as by the pannexin 1-blocking peptide ¹⁰Panx1 (Fig. 6). We further confirmed the involvement of the pannexin 1 hemichannel in the swelling-induced ATP release by using siRNA-mediated *Panx1* knockdown (Fig. 7). These data indicate that both the maxi-anion channel and the pannexin 1 hemichannel are involved in the ATP release from fibrosarcoma L929 cells.

Our present results supporting the role of pannexin 1 in the ATP release from fibrosarcoma cells are consistent with previous observations of a similar role for it in erythrocytes (28, 32, 37, 52), airway epithelial cells (39, 49), astrocytes (16, 21), ciliary epithelial cells (26), the pituitary gland (27), apoptotic lymphoid Jurkat cells (7), microglia, and neurons (35). As shown in Fig. 6, A and B, the inhibitory effect of a highly pannexin-specific blocker, ¹⁰Panx1 (by $8.4 \pm 1.7\%$), was less marked than the effect of probenecid (by $18.1 \pm 4.1\%$; $P = 0.04$) and looked less marked than that of mefloquine (by $16.4 \pm 3.8\%$; $P = 0.07$). Thus, it is possible that these nonspecific blockers inhibited some minor ATP release pathway other than pannexin 1. In contrast to pannexin 1, however, pannexin 2 plays no role in the ATP release, as we did not find any inhibitory effect of *Panx2*-specific siRNA treatment on the hypotonicity-induced ATP release (Fig. 8). Two different blockers of exocytosis, brefeldin A and bafilomycin A1, failed to inhibit the hypotonicity-induced ATP release from L929 cells, indicating that exocytosis does not play a role in the ATP release in these cells.

Connexin 43 and the maxi-anion channel are distinct entities in L929 cells. The connexin 43 hemichannel has long been under consideration as a possible pathway for the stimulated release of ATP in astrocytes (16, 35), microglia (35), cardiomyocytes (17, 48, 58, 59), and bovine ciliary epithelial cells (26). Therefore, a possible relationship between connexin 43 and the maxi-anion channel could be hypothesized, and in the present study, we attempted to test this possibility in L929 cells. We found that both the nonspecific connexin inhibitor 1-octanol and the connexin 43-specific peptide blocker Gap27 had no effect on maxi-anion channel activity (Fig. 9B). Moreover, the *Gjal* siRNA-mediated knockdown of connexin 43 had no effect on maxi-anion channel activity (Fig. 9D) even though connexin 43 mRNA expression was largely eliminated (Fig. 9C). Based on these data, we conclude that the maxi-anion channel and the connexin 43 hemichannel are distinct from each other.

A possible physiological function of swelling-induced ATP release. Released ATP may play a role in autocrine and/or paracrine cell-to-cell signaling via stimulation of purinergic receptors. ATP released from osmotically swollen cells has been shown to facilitate the process of RVD (6, 8, 10, 18, 34, 61). In L929 cells, it would be also the case, because their RVD ability was abolished by extracellular application of an ATP-hydrolyzing enzyme, apyrase (Fig. 4B, reversed triangles). The RVD response to hypotonic stimulation was also almost completely eliminated by Gd^{3+} (Fig. 4B, triangles). Thus, it appears that ATP released locally via Gd^{3+} -sensitive maxi-anion channels plays, in an autocrine manner, a facilitatory role in the cell volume regulation after osmotic swelling in L929 fibrosarcoma cells. In contrast, the RVD process was not significantly affected by probenecid (Fig. 4B, diamonds). Thus, it

may be inferred that probenecid-sensitive pannexin 1 hemichannels, which represent a minor pathway for ATP release (Fig. 6A), exist remote from purinergic receptors on the plasma membrane.

Conclusion. The maxi-anion channel and the pannexin 1 and connexin 43 hemichannels have been identified as possible ATP release pathways in different cell types. These channels are known to share some common biophysical and pharmacological properties. The present study, however, demonstrated that the maxi-anion channel is a distinct molecular entity from the pannexin 1 and connexin 43 hemichannels and that the maxi-anion channel and hemichannels serve as separate pathways for swelling-induced ATP release in murine L929 fibrosarcoma cells.

ACKNOWLEDGMENTS

We thank E. L. Lee for reading the manuscript, K. Shigemoto for technical assistance, and T. Okayasu for secretarial help.

GRANTS

This work was supported by Grant-in-Aid for Scientific Research to Y. Okada from the Japan Society for the Promotion of Science.

DISCLOSURES

No conflicts of interest, financial or otherwise, are declared by the author(s).

AUTHOR CONTRIBUTIONS

M.R.I., H.U., and T.O. performed the experiments; M.R.I., H.U., T.O., and R.Z.S. analyzed the data; M.R.I., H.U., and R.Z.S. prepared the figures; M.R.I. drafted the manuscript; R.Z.S. and Y.O. conception and design of the research; R.Z.S. and Y.O. interpreted the results of the experiments; R.Z.S. and Y.O. edited and revised the manuscript; Y.O. approved the final version of the manuscript.

REFERENCES

1. Akopova I, Tatur S, Grygorczyk M, Luchowski R, Gryczynski I, Gryczynski Z, Borejdo J, Grygorczyk R. Imaging exocytosis of ATP-containing vesicles with TIRF microscopy in lung epithelial A549 cells. *Purinergic Signal* 8: 59–70, 2012.
2. Ambrosi C, Gassmann O, Pranskevich JN, Boassa D, Smock A, Wang J, Dahl G, Steinem C, Sosinsky GE. Pannexin 1 and pannexin 2 channels show quaternary similarities to connexons and different oligomerization numbers from each other. *J Biol Chem* 285: 24420–24431, 2010.
3. Bao L, Locovei S, Dahl G. Pannexin membrane channels are mechanosensitive conduits for ATP. *FEBS Lett* 572: 65–68, 2004.
4. Bell PD, Lapointe JY, Sabirov R, Hayashi S, Peti-Peterdi J, Manabe KI, Kovacs G, Okada Y. Macula densa cell signaling involves ATP release through a maxi anion channel. *Proc Natl Acad Sci USA* 100: 4322–4327, 2003.
5. Boudreau F, Grygorczyk R. Cell swelling-induced ATP release and gadolinium-sensitive channels. *Am J Physiol Cell Physiol* 282: C219–C226, 2002.
6. Braunstein GM, Roman RM, Clancy JP, Kudlow BA, Taylor AL, Shylonsky VG, Jovov B, Peter K, Jilling T, Ismailov II, Benos DJ, Schwiebert LM, Fitz JG, Schwiebert EM. Cystic fibrosis transmembrane conductance regulator facilitates ATP release by stimulating a separate ATP release channel for autocrine control of cell volume regulation. *J Biol Chem* 276: 6621–6630, 2001.
7. Chekeni FB, Elliott MR, Sandilos JK, Walk SF, Kinchen JM, Lazowski ER, Armstrong AJ, Penuela S, Laird DW, Salvesen GS, Isakson BE, Bayliss DA, Ravichandran KS. Pannexin 1 channels mediate ‘find-me’ signal release and membrane permeability during apoptosis. *Nature* 467: 863–867, 2010.
8. Darby M, Kuzmiski JB, Panenka W, Feighan D, MacVicar BA. ATP released from astrocytes during swelling activates chloride channels. *J Neurophysiol* 89: 1870–1877, 2003.

9. De Vuyst E, Decrock E, Cabooter L, Dubyak GR, Naus CC, Evans WH, Leybaert L. Intracellular calcium changes trigger connexin 32 hemichannel opening. *EMBO J* 25: 34–44, 2006.
10. Dezaki K, Tsumura T, Maeno E, Okada Y. Receptor-mediated facilitation of cell volume regulation by swelling-induced ATP release in human epithelial cells. *Jpn J Physiol* 50: 235–241, 2000.
11. D'hondt C, Ponsaerts R, Smedt HD, Vinken M, Vuyst ED, Bock MD, Wang N, Rogiers V, Leybaert L, Himpens B, Bultynck G. Pannexin channels in ATP release and beyond: an unexpected rendezvous at the endoplasmic reticulum. *Cell Signal* 23: 305–316, 2011.
- 11a. Dubyak GR. Function without form: an ongoing search for maxi-anion channel proteins. Focus on "Maxi-anion channel and pannexin 1 hemichannel constitute separate pathways for swelling-induced ATP release in murine L929 fibrosarcoma cells." *Am J Physiol Cell Physiol* (August 29, 2012). doi:10.1152/ajpcell.00285.2012.
12. Dutta AK, Korchev YE, Shevchuk AI, Hayashi S, Okada Y, Sabirov RZ. Spatial distribution of maxi-anion channel on cardiomyocytes detected by smart-patch technique. *Biophys J* 94: 1646–1655, 2008.
13. Dutta AK, Okada Y, Sabirov RZ. Regulation of an ATP-conductive large-conductance anion channel and swelling-induced ATP release by arachidonic acid. *J Physiol* 542: 803–816, 2002.
14. Dutta AK, Sabirov RZ, Uramoto H, Okada Y. Role of ATP-conductive anion channel in ATP release from neonatal rat cardiomyocytes in ischemic or hypoxic conditions. *J Physiol* 559: 799–812, 2004.
15. Evans WH, Leybaert L. Mimetic peptides as blockers of connexin channel-facilitated intercellular communication. *Cell Commun Adhes* 14: 265–273, 2007.
16. Garré JM, Retamal MA, Cassina P, Barbeito L, Bukauskas FF, Sáez JC, Bennett MVL, Abudara V. FGF-1 induces ATP release from spinal astrocytes in culture and opens pannexin and connexin hemichannels. *Proc Natl Acad Sci USA* 107: 22659–22664, 2010.
17. Hawat G, Benderdour M, Rousseau G, Baroudi G. Connexin 43 mimetic peptide Gap26 confers protection to intact heart against myocardial ischemia injury. *Pflügers Arch* 460: 583–592, 2010.
18. Hazama A, Fan HT, Abdullaev I, Maeno E, Tanaka S, Ando-Akatsuka Y, Okada Y. Swelling-activated, cystic fibrosis transmembrane conductance regulator-augmented ATP release and Cl^- conductances in murine C127 cells. *J Physiol* 523: 1–11, 2000.
19. Hucklestep RT, id Bihi R, Eason R, Spyer KM, Dicke N, Willecke K, Marina N, Gourine AV, Dale N. Connexin hemichannel-mediated CO_2 -dependent release of ATP in the medulla oblongata contributes to central respiratory chemosensitivity. *J Physiol* 588: 3901–3920, 2010.
20. Iglesias R, Spray DC, Scemes E. Mefloquine blockade of Pannexin1 currents: resolution of a conflict. *Cell Commun Adhes* 16: 131–137, 2009.
21. Iwabuchi S, Kawahara K. Functional significance of the negative-feedback regulation of ATP release via pannexin-1 hemichannels under ischemic stress in astrocytes. *Neurochem Int* 58: 376–384, 2011.
22. Kienitz MC, Bender K, Dermietzel R, Pott L, Zoidl G. Pannexin 1 constitutes the large conductance cation channel of cardiac myocytes. *J Biol Chem* 286: 290–298, 2011.
23. Liu HT, Tashmukhamedov BA, Inoue H, Okada Y, Sabirov RZ. Roles of two types of anion channels in glutamate release from mouse astrocytes under ischemic or osmotic stress. *Glia* 54: 343–357, 2006.
24. Liu HT, Sabirov RZ, Okada Y. Oxygen-glucose deprivation induces ATP release via maxi-anion channels in astrocytes. *Purinergic Signal* 4: 147–154, 2008.
25. Liu HT, Toychiev AH, Takahashi N, Sabirov RZ, Okada Y. Maxi-anion channel as a candidate pathway for osmosensitive ATP release from mouse astrocytes in primary culture. *Cell Res* 18: 558–565, 2008.
26. Li A, Leung CT, Peterson-Yantorno K, Mitchell CH, Civan MM. Pathways for ATP release by bovine ciliary epithelial cells, the initial step in purinergic regulation of aqueous humor inflow. *Am J Physiol Cell Physiol* 299: C1308–C1317, 2010.
27. Li S, Bjelobaba I, Yan Z, Kucka M, Tomic M, Stojilkovic SS. Expression and roles of pannexins in ATP release in the pituitary gland. *Neuroendocrinology* 152: 2342–2352, 2011.
28. Locovei S, Bao L, Dahl G. Pannexin 1 in erythrocytes: function without a gap. *Proc Natl Acad Sci USA* 103: 7655–7659, 2006.
29. Ma W, Hui H, Pelegrin P, Surprenant A. Pharmacological characterization of pannexin-1 currents expressed in mammalian cells. *J Pharmacol Exp Ther* 328: 409–418, 2009.
30. MacVicar BA, Thompson RJ. Non-junction functions of pannexin-1 channels. *Trends Neurosci* 33: 93–102, 2009.
31. Maleszka R, Hanes SD, Hackett RL, de Couet HG, Miklos GL. The *Drosophila melanogaster* dodo (*dod*) gene, conserved in humans, is functionally interchangeable with the ESS1 cell division gene of *Saccharomyces cerevisiae*. *Proc Natl Acad Sci USA* 93: 447–451, 1996.
32. Montalbetti N, Leal Denis MF, Pignataro OP, Kobatake E, Lazarski ER, Schwarzbaum PJ. Homeostasis of extracellular ATP in human erythrocytes. *J Biol Chem* 286: 38397–38407, 2011.
33. Okada Y, Sato K, Toychiev AH, Suzuki M, Dutta AK, Inoue H, Sabirov RZ. The puzzles of volume-activated anion channels. In: *Physiology and Pathology of Chloride Transporters and Channels in the Nervous System: From Molecules to Diseases*, edited by Alvarez-Leefmans FJ, Delpire E. San Diego, CA: Elsevier, 2009.
34. Okada Y, Maeno E, Shimizu T, Dezaki K, Wang J, Morishima S. Receptor-mediated control of regulatory volume decrease (RVD) and apoptotic volume decrease (AVD). *J Physiol* 532: 3–16, 2001.
35. Orellana JA, Shoji KF, Abudara V, Egan P, Amigou E, Sáez JC, Jiang JX, Naus CC, Sáez JC, Giaume C. Amyloid β -induced death in neurons involves glial and neuronal hemichannels. *J Neurosci* 31: 4962–4977, 2011.
36. Pelegrin P, Surprenant A. Pannexin-1 mediates large pore formation and interleukin-1 β release by the ATP-gated P2X_7 receptor. *EMBO J* 25: 5071–5082, 2006.
37. Qiu F, Wang J, Spray DC, Scemes E, Dahl G. Two non-vesicular ATP release pathways in the mouse erythrocyte membrane. *FEBS Lett* 585: 3430–3435, 2011.
38. Ramsingh R, Grygorczyk A, Solecki A, Cherkaoui LS, Berthiaume Y, Grygorczyk R. Cell deformation at the air-liquid interface induces Ca^{2+} -dependent ATP release from lung epithelial cells. *Am J Physiol Lung Cell Mol Physiol* 300: L587–L595, 2011.
39. Ransford GA, Fregien N, Qiu F, Dahl G, Conner GE, Salathe M. Pannexin 1 contributes to ATP release in airway epithelia. *Am J Respir Cell Mol Biol* 41: 525–534, 2009.
40. Roman RM, Feranchak AP, Davison AK, Schwiebert EM, Fitz JG. Evidence for Gd^{3+} inhibition of membrane ATP permeability and purinergic signalling. *Am J Physiol Gastrointest Liver Physiol* 277: G1222–G1230, 1999.
41. Sabirov RZ, Dutta AK, Okada Y. Volume-dependent ATP-conductive large-conductance anion channel as a pathway for swelling-induced ATP release. *J Gen Physiol* 118: 251–266, 2001.
42. Sabirov RZ, Merzlyak PG. Plasmalemmal VDAC controversies and maxi-anion channel puzzle. *Biochim Biophys Acta* 1818: 1570–1580, 2012.
43. Sabirov RZ, Okada Y. Wide nanoscopic pore of maxi-anion channel suits its function as an ATP-conductive pathway. *Biophys J* 87: 1672–1685, 2004.
44. Sabirov RZ, Okada Y. ATP-conducting maxi-anion channel: a new player in stress-sensory transduction. *Jpn J Physiol* 54: 7–14, 2004.
45. Sabirov RZ, Okada Y. ATP release via anion channels. *Purinergic Signal* 1: 311–328, 2005.
46. Sabirov RZ, Okada Y. The maxi-anion channel: a classical channel playing novel roles through an unidentified molecular entity. *J Physiol Sci* 59: 3–21, 2009.
47. Sabirov RZ, Sheiko T, Liu H, Deng D, Okada Y, Craigen WJ. Genetic demonstration that the plasma membrane maxianion channel and voltage-dependent anion channels are unrelated proteins. *J Biol Chem* 281: 1897–1904, 2006.
48. Scemes E, Spray DC, Meda P. Connexins, pannexins, innexins: novel roles of "hemi-channels". *Pflügers Arch* 457: 1207–1226, 2009.
49. Seminario-Vidal L, Okada SF, Sesma JI, Kreda SM, van Heusden CA, Zhu Y, Jones LC, O'Neal WK, Penuela S, Laird DW, Boucher RC, Lazarski ER. Rho signaling regulates pannexin 1-mediated ATP release from airway epithelia. *J Biol Chem* 286: 26277–26286, 2011.
50. Silverman WR, de Rivero Vaccari JP, Locovei S, Qiu F, Carlsson SK, Scemes E, Keane RW, Dahl G. The pannexin 1 channel activates the inflammasome in neurons and astrocytes. *J Biol Chem* 284: 18143–18151, 2009.
51. Silverman W, Locovei S, Dahl G. Probenecid, a gout remedy, inhibits pannexin 1 channels. *Am J Physiol Cell Physiol* 295: C761–C767, 2008.
52. Sridharan M, Adderley SP, Bowles EA, Egan TM, Stephenson AH, Ellsworth ML, Sprague RS. Pannexin 1 is the conduit for low oxygen tension-induced ATP release from human erythrocytes. *Am J Physiol Heart Circ Physiol* 299: H1146–H1152, 2010.

53. Su AI, Cooke MP, Ching KA, Hakak Y, Walker JR, Wiltshire T, Orth AP, Vega RG, Sapinoso LM, Moqrich A, Patapoutian A, Hampton GM, Schultz PG, Hogenesch JB. Large-scale analysis of the human and mouse transcriptomes. *Proc Natl Acad Sci USA* 99: 4465–4470, 2002.
54. Suzuki M, Mizuno A. A novel human Cl^- channel family related to *Drosophila* flightless locus. *J Biol Chem* 279: 22461–22468, 2004.
55. Suzuki M. The *Drosophila* tweety family: molecular candidates for large-conductance Ca^{2+} -activated Cl^- channels. *Exp Physiol* 91: 141–147, 2006.
56. Tatur S, Groulx N, Orlov SN, Grygorczyk R. Ca^{2+} -dependent ATP release from A549 cells involves synergistic autocrine stimulation by coreleased uridine nucleotides. *J Physiol* 584: 419–435, 2007.
57. Tatur S, Kreda S, Lazarowski E, Grygorczyk R. Calcium-dependent release of adenosine and uridine nucleotides from A549 cells. *Purinergic Signal* 4: 139–146, 2008.
58. Thompson RJ, Zhou N, MacVicar BA. Ischemia opens neuronal gap junction hemichannels. *Science* 312: 924–927, 2006.
59. Thompson RJ, MacVicar BA. Connexin and pannexin hemichannels of neurons and astrocytes. *Channels (Austin)* 2: 81–86, 2008.
60. Toychiev AH, Sabirov RZ, Takahashi N, Ando-Akatsuka Y, Liu H, Shintani T, Noda M, Okada Y. Activation of maxi-anion channel by protein tyrosine dephosphorylation. *Am J Physiol Cell Physiol* 297: C990–C1000, 2009.
61. Wang Y, Roman R, Lidofsky SD, Fitz JG. Autocrine signaling through ATP release represents a novel mechanism for cell volume regulation. *Proc Natl Acad Sci USA* 93: 12020–12025, 1996.
62. Xu XJ, Boumechache M, Robinson LE, Marschall V, Gorecki DC, Masin M, Murrell-Lagnado R. Splice-variants of the P2X7 receptor reveal differential agonist-dependence and functional coupling with pannexin-1. *J Cell Sci*. In press.

